

The Feasibility of Dense Indoor LoRaWAN Towards Passively Sensing Human Presence

Jascha Grübel*, Tyler Thrash[†], Didier H elal[‡], Robert W. Sumner*, Christoph H olscher*, Victor R. Schinazi[§]

* ETH Z urich, Z urich, Switzerland

Email: jascha.gruebel@inf.ethz.ch, robert.sumner@inf.ethz.ch, christoph.hoelscher@gess.ethz.ch

[†] Miami University, Oxford, OH, USA

Email: thrashst@miamioh.edu

[‡] Orbiwise, Geneva, Switzerland

Email: didier.helal@orbiwise.com

[§] Bond University, Robina, Australia

Email: victor_schinazi@bond.edu.au

Abstract—Long Range Wide Area Network (LoRaWAN) has been advanced as an alternative for creating indoor sensor networks that extends beyond its original long-distance communication purpose. For the present paper, we developed a Dense Indoor Sensor Network (DISN) with 390 sensor nodes and three gateways and empirically evaluated its performance for half a year. Our analysis of more than 14 million transmissions revealed that DISNs achieve a much lower distance coverage compared to previous research. In addition, the deployment of multiple gateways decreased the loss of transmissions due to environmental and network factors such as concurrently received messages. Given the complexity of our system, we received few colliding concurrent messages, which demonstrates a gap between the projected requirements of LoRaWAN systems and the actual requirements of real-world applications. Our attenuation model indicates that robust coverage in an indoor environment can be maintained by placing a gateway every 30 m and every 5 floors. We discuss the application of DISNs for the passive sensing and visualization of human presence using a Digital Twin (DT).

I. INTRODUCTION

A Dense Indoor Sensor Network (DISN) based on Low Power Wide Area Networks (LPWAN) provides opportunities to estimate human presence in the wild. Originally, LPWANs were developed to cover large outdoor distances with a robust signal at low cost [1]–[6]. In a LPWAN setup, devices are not easily accessible and must operate with limited maintenance, without external energy supply, and with limited capacity for data transmission. Notably, the features of LPWAN that enable robust long-distance outdoor communication are also attractive indoors because of the low additional overhead for existing infrastructure and easier management of densely crowded bandwidth. One drawback of LPWAN implementations is a low Data Rate (DR) that may be further diminished in order to increase signal quality.

The most common LPWAN standard is Long Range Wide Area Network (LoRaWAN) [7]. LoRaWAN is gaining attention [8] in both research and industry for three reasons. First, LoRaWAN is an open standard, and the only proprietary component from Semtech is a low-cost LoRa transceiver (LoRa PHY) [7]. LoRa PHY encodes information with a

chirp spread spectrum [9] and an integrated forward error correction (FEC) [10] as specified under IEEE802.15.4a [11]. Second, LoRaWAN uses the unlicensed industrial, scientific, and medical (ISM) frequency bands in contrast to expensive cellular networks. The unlicensed spectrum is free to use but regulated, and in Europe, the spectrum has a duty cycle limitation of 1% [12]. Third, LoRaWAN is reliable and easy to use due to its design. A battery life of 10 years is possible with LoRaWAN class A sensor nodes because of an asymmetrical uplink communication from sensor to server with an ALOHA-like [13] time window for uplink communication followed by a dedicated downlink time window [7].

In typical applications, LoRa PHY can send data over distances of 10–40 km in rural areas, 1–5 km in urban areas [15], and less than 200 m in dense urban areas [24]. The spreading factor (SF) determines the reliability of the transmission and the time to broadcast the chirp signal [7]. The SF varies from 7 to 12 with higher values representing a more robust signal and reduced bandwidth [10]. At the best possible DR, only low bandwidth (0.3–50 kb/s) applications [10] are feasible. Theoretically, millions of devices can be supported within a single LoRaWAN network because of the star-of-star topology [15]. However, there is a trade-off between the number of devices and the number of transmissions which is imposed by the duty cycle limitation and interference from colliding concurrent messages [21].

By allowing for DISNs, LoRaWAN may be suitable for studying human presence at a high spatiotemporal resolution [25]. Indoor human presence can be measured actively or passively [26]. Whereas active tracking requires participants to wear sensors [27], passive tracking infers human presence from changes in environmental factors measured by stationary sensors [28]. Usually, a single sensor per room is used to measure human presence as an indication of occupancy [28]. Inferring human presence can be facilitated with a Digital Twin (DT) [29], [30] underpinned by LoRaWAN as a Service-oriented Architecture (SoA) [31] middleware. A DT is a platform for digitally mirroring processes from the physical

TABLE I
LoRaWAN INDOOR STUDIES

	[14]	[15]	[16]	[17]	[18]	[19]	[20]	[21]	[22]	[23]
Region	Europe	Europe	Europe	Europe	Europe	Asia	Europe	Europe	Asia	Europe
#Floors	1	19	9	8	1	5	4	6	-	1
Distances	103 m	-	ca. 20 m	ca. 100 m	190 m	-	60 m	420 m	150 m	-
Data rate (SF) [†]	all	auto	all	12	7/12	all	all	all	11	9/10/12
Gateways	1	1	1	1	1	1	1	1	1	1
Devices	4	32	1	1	2	5	1	1	1	1
Locations	4	32	13	-*	46	5	13	23	4	4
Transmissions	50	-	1200	-	50	-	80 hours	600	60	-

[†] All DRs used BW125; * Only a heat map was shown.

world [32]–[34] that is suitable for continuously evaluating human presence indoors [35]. In general, empirical testbeds for LoRaWAN with a large number of sensors are scarce [36], although recently, an outdoor scenario with 50 nodes was tested [37]. Nonetheless, many questions on the scalability of LoRaWAN remain open, especially for DISNs, including the number of sensor nodes that are feasible indoors, the attenuation of the signal by the environment (e.g., walls, floors), and the feasibility of LoRaWAN as part of a continuously running system.

The present paper is the first to demonstrate the technical feasibility of a LoRaWAN DISN with 390 nodes and 3 gateways in an office building. Our DISN is capable of maintaining a strong signal on all DR at distances up to 30 m and 5 floors for a single gateway. At the lowest DR, theoretical distances up to 150 m are possible, but each additional floor halves this distance, limiting sensible setups to 5 floors. With 390 sensors on 8 floors and up to 64 m of distance from sensor to gateway, the system received an average of 55000 transmissions daily. The percent of concurrent messages (i.e., on different channels and spreading factors) was 5.5%, but the percent of colliding concurrent messages (i.e., on the same channel and spreading factor) was negligible at 0.29%. The 3 gateways allowed us to reduce the Frame Error Rate (FER) by 37.5% compared to the best performing gateway. We report much lower maximal distances and show that previous work on indoor LoRaWAN networks was optimistic, but multiple gateways may compensate for this shortcoming.

II. RELATED WORK

Despite the original application of LoRaWAN outdoors, researchers have investigated LoRaWAN indoors (see Table I) using a minimal viable design (e.g., one gateway, one device, and one network server) and therefore could not measure performance with multiple sensors [16], [17], [20]–[22]. In these studies, the device was moved to multiple locations within the building, mostly on the same floor [16], [20], [21]. In addition, many of these models were based on simulations and were never implemented with multiple sensors [18]. Despite these limitations, research suggests that higher DRs can work indoors without sacrificing connectivity coverage [20].

Typically, signal quality is measured either as the Signal to Noise Ratio (SNR) or the Received Signal Strength Indicator

(RSSI). SNR indicates whether a message can be received at all. In other transmission technologies, the noise floor is usually at 0 db beyond which demodulation cannot occur. However, LoRa allows for a lower noise floor at which messages are lost between -7.5 db and -20 db because of chirp signal modulation [10]. RSSI can indicate the level at which the signal weakens, which strongly depends on the transceiver. A general convention is that signals at -60 dbm are considered strong and below -100 dbm are considered weak [38].

Previous studies have found that a single gateway has reasonable coverage indoors and that the signal can remain stable for buildings up to 4 floors [16], [20]. In addition, they found no discernible effect of placing the sensor nodes on different floors with the exception of the basement where the signal deteriorated quickly. Indeed, in reinforced concrete buildings the signal attenuates quickly covering 8 floors and approximately 100 m [17], [23]. Together, these studies suggest that a higher SF is critical for traversing denser materials.

In other scenarios, gateways installed above low-rise buildings without reinforced materials, which allowed for transmissions up to 420 m [21]. In contrast, gateways installed in an open floor could receive transmissions up to 190 m [18]. Only a few studies have investigated distances longer than 100 m, and it is unknown whether interference within buildings reaches a threshold by which an additional gateway must be placed. To our knowledge, no study has determined the distance limits of indoor transmissions or offered a limit on the number of floors that a single gateway can cover.

III. SYSTEM DESIGN & IMPLEMENTATION

Our LoRaWAN DISN forms the basis for a DT to represent physically-based higher order processes [32] necessary to investigate human presence. We map the DT to a classicist three-layer Internet of Things (IoT) architecture [39] (see Fig.1), including (1) data collection, (2) transmission, and (3) utilization (see Fig. 2).

A. Data collection

The data collection layer collects environmental characteristics containing passively observable data on human presence in a public building. We tested our LoRaWAN-based DT on an 8 floor office building at ETH Zürich (ETHZ). The public part of the building consists of 5 floors with a small lecture

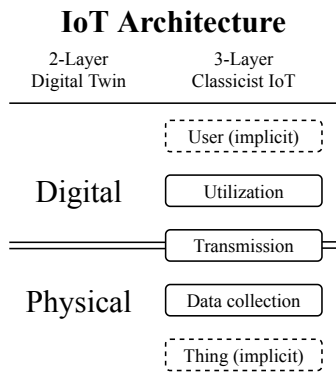







Fig. 1. Abstract system architecture. The digital twin [32] (left) maps to the implementation model [39] (right). Implicit layers (*Things* that sense and *Users* that operate) are also shown in dashed boxes.

hall on the 1st floor (see Fig. 3). We placed 390 sensors in 19 distinct rooms of varying sizes that may exhibit different levels of human presence (see Fig. 4).

Each of the five types of battery-powered sensor nodes uses LoRa PHY for communication and was selected to cover typical indicators of human presence, including temperature, CO₂-levels [42], noise [43], humidity, and motion [44] (see Table II). We focused on sensors that covered CO₂ (40 nodes) and Volatile Organic Compounds (VOC; 40 nodes) as lingering effects of human presence. We also employed noise sensors (40 nodes) and motion sensors (250 nodes) that immediately indicate presence but are susceptible to false positives. In addition, we collected environmental factors (e.g., temperature, humidity, brightness) that can be driven both by human presence and other factors such as weather, heating, time of day, and whether outside windows and doors are open.

TABLE II
SELECTED SENSORS FOR THE PROTOTYPE AT THE UNIVERSITY.

	ERS CO ₂	ERS	Orbiwise Sampol	Browan Tabs IAQ	Browan Tabs
					
CO ₂	✓			✓	
VOC				✓	
PIR Motion	✓	✓			✓
Brightness	✓	✓		✓	✓
Noise			✓		
Humidity	✓	✓	✓	✓	✓
Temperature	✓	✓	✓	✓	✓
Focus	Motion	CO ₂	Sound	VOC	Motion
Sample rate	10 min	10 min	5 min	5 min	Event
Bandwidth	125 kHz	125 kHz	125 kHz	125 kHz	125 kHz
Count	60	40	40	40	210

The placement of sensors needs to conform to several requirements and was stored for analysis. First, sensors can only collect data in public spaces including staircases, hallways, and auditoriums. The privacy of building users was maintained as sensors were not placed in offices, bathrooms, or other

private areas. Second, sensors should be well-distributed to support data fusion. Sensors of the same type were densely and uniformly placed throughout each room. Third, sensors must be placed within the limitations of the existing building. The sensors are mounted on the ceiling beyond the reach and attention of building users while accounting for the other hardware, including cable trays and WiFi-routers.

B. Transmission

The sensor data is made available with a SoA design by which each processing step is performed independently to increase interoperability. The data from the sensors are sent to the network server, stored persistently on a database server, and made accessible for further analysis in the DT (see Fig. 2). All sensors are configured as Class A LoRaWAN devices [7] that collect data every 5 to 10 minutes or event-based (see Table II). The sensors transmit their payload to the gateways on a channel with a bandwidth of 125 kHz secured with AES-128 [7]. Re-transmission was disabled to prolong the battery life at the cost of missing some transmissions due to collisions.

Our LoRaWAN network has two gateways placed on the ground floor of the public part of the building and one gateway placed several floors below on the ground floor of the adjacent non-public part of the building (shown in green in Fig. 4). We use orbiLINK v4 indoor LoRaWAN nano-gateways (max. 27 dBm; class A & C devices; 8 LoRa channels) [45]. The gateway converts the IEEE 64-bit extended unique identifier (EUI) [7] to a IPv4 address and forwards it to a proprietary LoRaWAN network server.

The network server sets the Adaptive Data Rate (ADR), enforces the Link Adaptation Policy (LAP), forwards the payload, and synchronizes the gateway clocks (delay <20 ms). Our network server performs a two-step optimization based on ADR and LAP to optimize the available bandwidth, comply with duty cycles, save battery life, and reduce Time-on-Air (ToA). For the ADR step, the SF is adjusted whenever the average of the last 15 transmissions crosses the SF threshold with a 12 db margin, see Table III. Switching the SF resets transmission power to the maximal output to ensure that a link can be established. For the LAP step, the transmission power is reduced such that transfers occur barely above the noise level. In practice, LAP is only applied on SF7 because there is usually no power budget available for higher SF. The payload is decrypted with an application key [7], combined with meta-data from each gateway (e.g., SNR and RSSI), and converted into JavaScript Object Notation (JSON). The network server provides a webhook (HTTP push API) secured with basic access authentication (HTTP Auth) and immediately pushes the JSONs to our persistent storage facility.

The persistent storage facility *Experiments in Virtual Environments Representational State Transfer* (EVEREST) that extends the larger open-source platform EVE [40] and forms a core feature of the DT. EVEREST is a flask-based python server that implements Representational State Transfer Hypertext Application Language (REST-HAL) [46]. The webhook consumes all messages from the network server and inserts

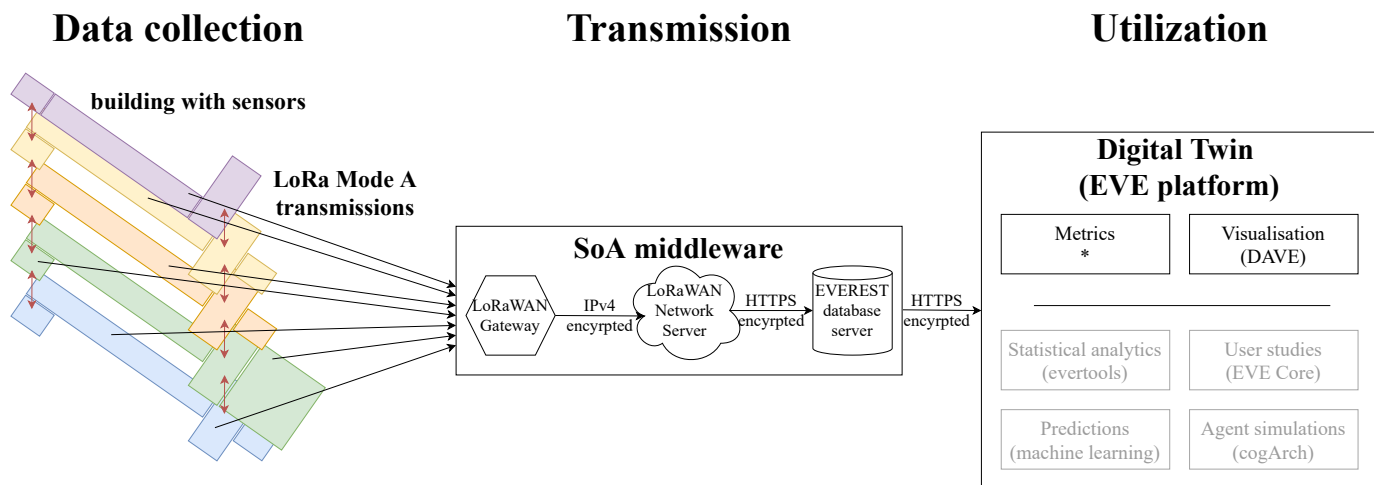


Fig. 2. Implemented system architecture. LoRaWAN sensors in the building configured in LoRa mode A (left). Gateways forward data to a network server which pushes them to the database EVEREST (center). In the DT, data is loaded from the SoA middleware EVEREST to view metrics and visualizations. Planned features (shown in gray) include statistical analysis, user studies based on EVE [40], predictions, and agent-based simulations [41] (right).

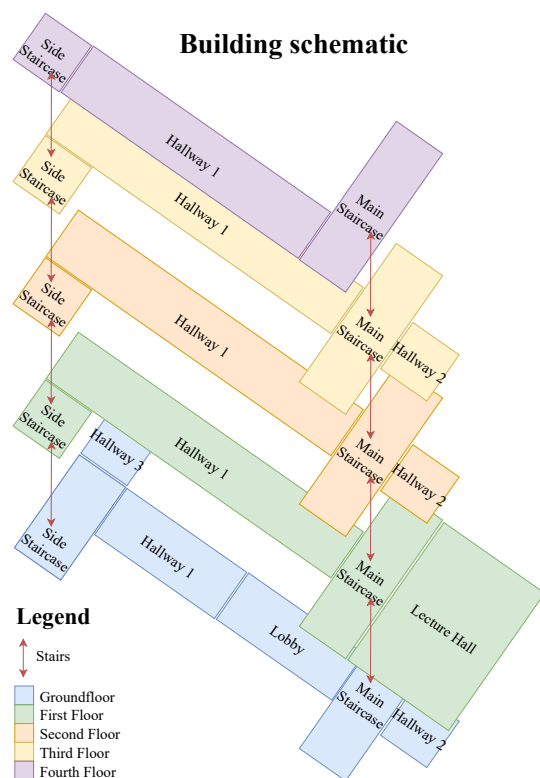


Fig. 3. A schematic layout of the public part of the building with stairs as red arrows.

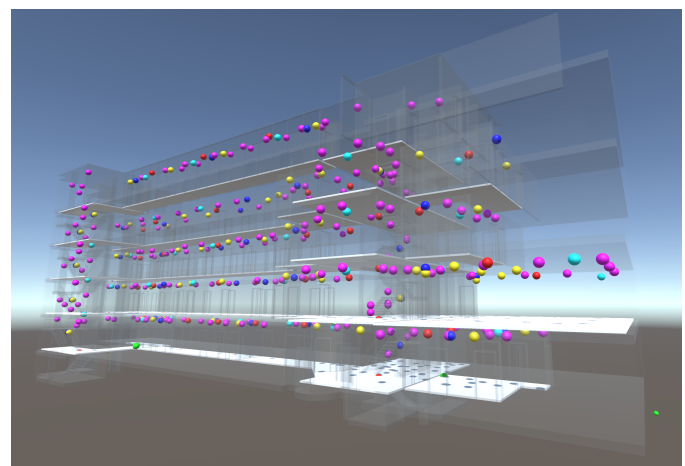


Fig. 4. The 390 sensors shown in DAVE with white rectangles for the involved rooms. The gateways are green (one is in the non-public area of the building, 3 floors down in the bottom right corner). Different types of sensors are represented as spheres of different colors (noise: blue; CO₂: red; VOC: cyan; PIR: yellow and magenta).

TABLE III
THE SNR THRESHOLDS FOR THE ADR ALGORITHM.

SF	Decrease Threshold	Increase Threshold
SF7	*	-7.5
SF8	-5	-10
SF9	-7.5	-12.5
SF10	-10	-15
SF11	-12.5	-17.5
SF12	-15	*

*Cannot increase or decrease further. Margins are not included.

the data into a local PostgreSQL database extended with TimescaleDB for time-series and Postgis for spatial data. Finally, the EVEREST server is hosted on a virtual machine with 4 virtual processors and 32 GB RAM at ETHZ.

C. Utilization

The utilization layer consists of a prototype of the visual DT, which is also integrated into the EVE platform [40]. The DT can be explored using an add-on called Data Analytics in

Virtual Environments (DAVE; see Fig. 4). Because readings from any single sensor would be difficult to interpret, a building information model (BIM) in DAVE provides spatial context for the densely placed sensors. Our DT also includes features for visualization and analysis (see Fig. 5). The data is stored on EVEREST in near-real time and immediately displayed in the DT. The difference to real time display is due to a tradeoff between power usage and transmission delay in the transmission settings of LoRaWAN because of limited battery life of the sensors.

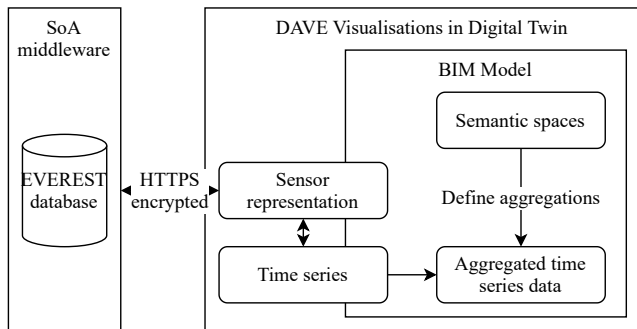


Fig. 5. The processing pipeline of sensor data in our DT implemented in the EVE platform. Sensor data is delivered by the SoA middleware EVEREST.

IV. RESULTS

Between March and July 2020, our setup collected 14 million transmissions over a range of up to 64 m and 8 Floors. ADR allowed us to analyze the preferred channel in our setup. The majority of messages were sent on SF7 (92.6%; see Fig. 6). Given the short maximal distance, we expected all gateways to receive a similar amount of transmissions. The two gateways located in the public part of the building received a similar amount of messages (see Fig. 7). The gateway located in the non-public part of the building only received between one and two magnitudes fewer transmissions depending on the originating floor. In addition, as the number of floors increases, ADR increases the SF to compensate for the loss of messages. We calculated the FER from the sequence number of the received JSON such that any jump in the sequence indicates a lost frame.

Overall, the two public gateways reported an FER of 25.51% and 17.46%, while the remote gateway reported an FER of 80.55% (see Fig. 8). The average FER reported at the network server across all sensor nodes was 8.06% which is considerably lower than any individual gateway's FER because some frames only arrive at one gateway and appear lost for the other gateways but can be restored from the network perspective (see Fig. 8). Note that our FER includes frames lost due to gateways being disconnected from the network. No sensor reported a duty cycle usage higher than 0.004%. No more than 5 colliding concurrent messages occurred on the same SF and channel with more than 99.7% of messages reporting no collision (see Fig. 9).

We analyzed the signal quality of LoRaWAN transmissions in terms of SNR and RSSI. First, we observed the SNR and

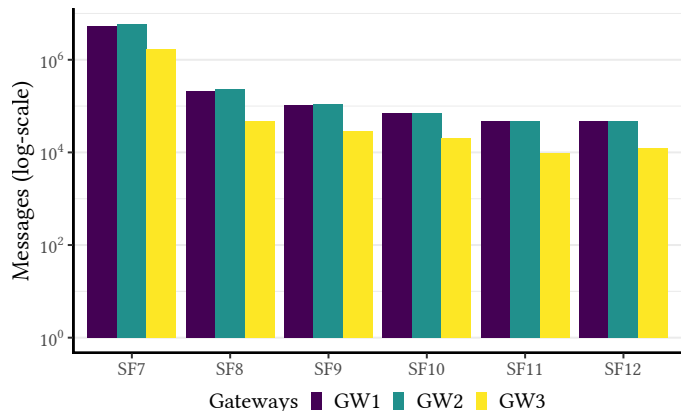


Fig. 6. The spreading factor (SF) and bandwidth (BW) of all received transmissions at each gateway (GW) on a log-scale.

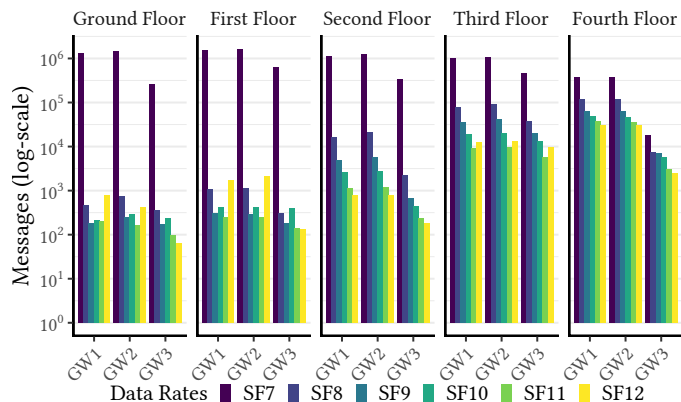


Fig. 7. Received transmissions per GW, floor, and SF on a log-scale. Each transmission can arrive at all GWs. Higher SF are more often used in higher floors.

RSSI grouped by DR and the number of floors between the sensor nodes and the gateway. Next, we plotted these grouped measures as functions of the distance between sensor node and gateway (see Fig. 10). We observed a clear decay of the signal with increasing distance and number of floors across all DR, indicating attenuation that occurs beyond physical path loss models for open space [47]. However, the effect of floors on signal quality decreases with distance. Because most data were sent on SF7, SF7 produced the most stable curve. Higher SF seemed to offer some signal stability for very short distances but quickly deteriorated and approached the noise floor of LoRa at 30 m. Note that higher SF started with a higher SNR and RSSI for short distances because ADR resets the power output. While higher SFs increase ToA and allow the signal to be integrated, leading to higher SNR and RSSI [14], they are also more prone to signal shadowing and multi-path fading indoors [14]. This may explain why signal strength in our study quickly reached the noise floor.

We modeled attenuation as linear signal decay to understand the relations among distance, building structure, indoor obstacles, and network. Because each of the 390 sensors regularly sent transmissions, signal strength was not independent. We

TABLE IV
MIXED MODELS TO DETERMINE SNR AND RSSI FOR EACH DATA RATE

	SF7		SF8		SF9		SF10		SF11		SF12	
	SNR	RSSI	SNR	RSSI	SNR	RSSI	SNR	RSSI	SNR	RSSI	SNR	RSSI
Average signal strength at node (constant)	10.03* (0.09)	-63.75* (0.46)	10.35* (0.23)	-94.75* (0.61)	10.00* (0.29)	-97.33* (0.64)	8.07* (0.35)	-87.07* (0.91)	10.45* (0.36)	-85.05* (0.90)	8.38* (0.43)	-60.35* (0.77)
Attenuation in m	-0.27* (0.00)	-1.61* (0.00)	-0.43* (0.00)	-0.49* (0.00)	-0.44* (0.00)	-0.45* (0.00)	-0.32* (0.00)	-0.55* (0.00)	-0.34* (0.01)	-0.61* (0.01)	-0.20* (0.01)	-1.09* (0.01)
One floor between	-0.26* (0.00)	-9.48* (0.01)	0.04 (0.03)	-1.92* (0.03)	-0.92* (0.04)	-2.89* (0.03)	-0.96* (0.05)	-5.29* (0.04)	-2.50* (0.07)	-7.10* (0.06)	-2.68* (0.08)	-14.86* (0.08)
Floor-attenuation interaction	-0.01* (0.00)	0.29* (0.00)	0.02* (0.00)	0.07* (0.00)	0.04* (0.00)	0.08* (0.00)	0.02* (0.00)	0.12* (0.00)	0.04* (0.00)	0.15* (0.00)	0.02* (0.00)	0.29* (0.00)
Colliding message	0.13* (0.01)	1.57* (0.05)	0.17 (0.28)	0.67 (0.28)	0.24 (0.44)	0.66 (0.34)	0.77 (0.43)	0.36 (0.36)	1.37* (0.29)	0.27 (0.25)	0.63 (0.21)	0.27 (0.21)
Observations	12,948,936	12,948,936	495,967	495,967	246,184	246,184	160,618	160,618	104,499	104,499	106,025	106,025

*p<0.001

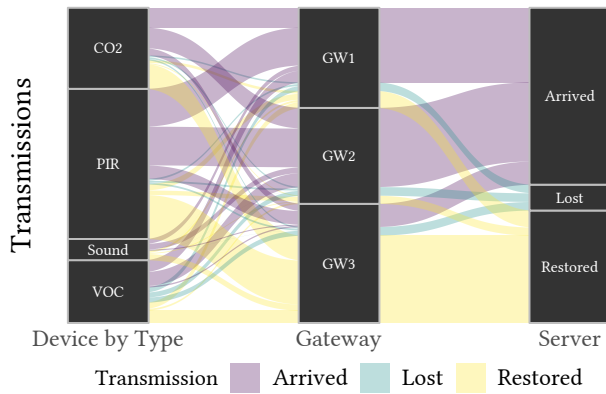


Fig. 8. FER by gateways and devices. Transmissions are aggregated by device type (right), gateways (middle) and the network server (left). Transmissions are represented by different colors (purple: arrived; green: lost; yellow: restored). Restored messages arrived at least at one gateway and could be restored for other gateways substantially reducing lost transmissions. Each transmission is counted thrice to account for it passing at each gateway. The overall proportion of arrived, lost, and restored messages remains unchanged.

used a mixed model [48] to quantify the impact of the structural setup on SNR and RSSI. This allowed us to account for the dependence among multiple transmissions from each sensor by modeling transmissions nested within sensor nodes. To better understand the impact of DRs on SNR and RSSI, we created independent models for each SF. Our models have fixed effects for environmental criteria (i.e., distance and number of floors) and network criteria (i.e., colliding concurrent messages) and random intercepts for each sensor (see Eq. 1). We computed SNR and RSSI as the output y for a regression on fixed effects at every transmission j and sensor i . The coefficients b group the q transmissions that each sensor i sent and represent the random intercept. For the concurrent message variable, we counted the number of other transmissions that were “on air” during a transmission. We subtracted the ToA from the gateway timestamp to define the interval in which arriving messages overlapped at different

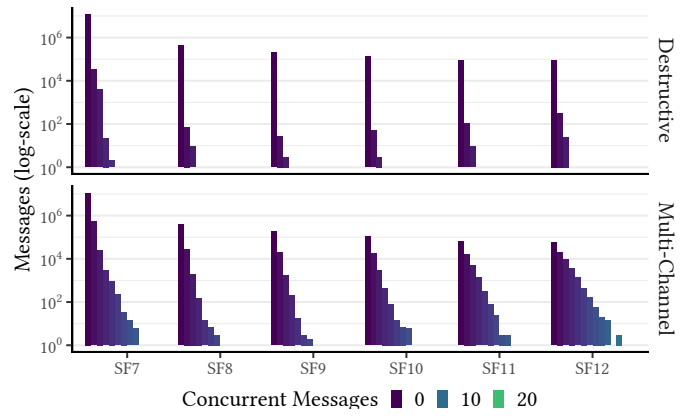


Fig. 9. Summary of concurrent transmissions being received in the same time window. Destructive concurrent transmissions are received on the same SF and channel at different GWs (top) whereas multi-channel transmissions are received on all SF and channels at all GWs (bottom). Many transmissions occur in the same time window but only a fraction of them are destructive such that they would not have been received at all if there was only one gateway.

gateways on the same SF and channel. In addition, this interval was expanded by 25% on each side to produce a time window that accounts for the gateway synchronization delay. Because complex physical simulations would be necessary to account for signal shadowing and multi-path fading, the distance variable (meters from gateway to sensor nodes) accounts for physical “path loss” as a black-box linear factor that covers different covarying environmental aspects. This approach substantially differs from classical LoRaWAN models based only on free space path loss [47].

$$y_{ij} = \beta_0 + \beta_1 \text{distance}_{ij} + \beta_2 \text{floor}_{ij} + \beta_3 \text{distance}_{ij} * \text{floor}_{ij} + \beta_4 \text{concurrent}_{ij} + b_{i1} z_{1ij} + \dots + b_{iq} z_{qij} + \epsilon_{ij} \quad (1)$$

Our models (see Table IV) confirmed the expectations derived from the descriptive data. The models’ constants indicated average signal strengths at the sensor node of around

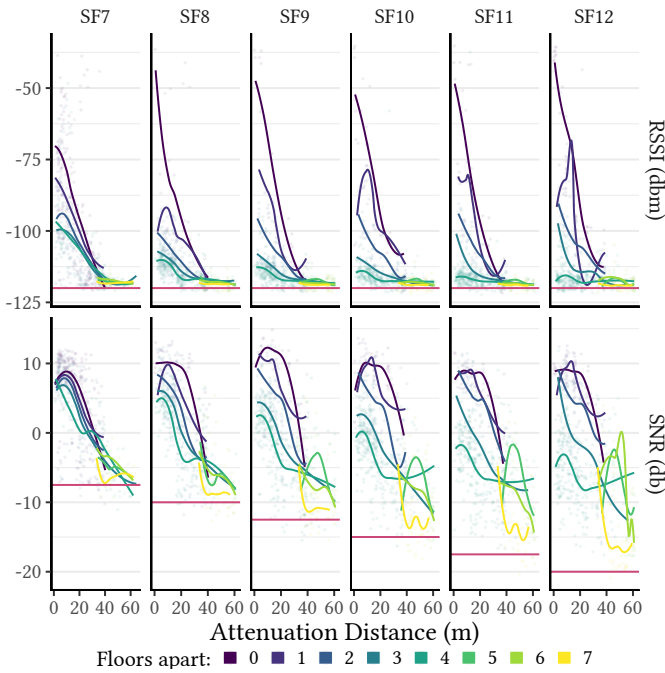


Fig. 10. The SNR and RSSI as a function of distance given the DR. The red horizontal line indicates the noise floor threshold of LoRaWAN. For SNR, the threshold depends on the DR [10], and for RSSI, the -121 dbm threshold depends on the gateway. The curves are aggregated SNR and RSSI measures based on locally estimated scatterplot smoothing (LOESS) regression. The points represent a random sample of real measurements to display the underlying distribution.

9 ± 1 db for SNR and -79 ± 19 dbm for RSSI. Here, we discuss SF7 in detail because it represented most messages. Due to attenuation, our SNR model predicted a signal loss of -0.270 db per meter. In addition, our RSSI model predicted a signal loss of -1.609 dbm per meter. Given that the height of each floor in the building was 3.36 m, we estimated that each floor affected the signal strength by -1.183 db (SNR) and -13.908 dbm (RSSI). These interactions between attenuation distance and the number of floors were significant for SNR and RSSI. While these interactions for the SNR model were small and negative, they were substantial and positive for the RSSI model, indicating that the signal was becoming weaker at a slower rate as the number of floors increased. Concurrent transmission occurred so seldom that the improvement in the signal of 0.128 db (SNR) and 1.573 dbm (RSSI) appeared to be an artifact.

To compare all SF, it is necessary to interpret the models' coefficients in terms of limits for transmission (see Table V). Here, we indicate the maximal distances that our system would support according to our model. Under ADR, sensor nodes on SF7 communicate with less transmission power than would be possible otherwise (to conserve battery), which may explain why SF7 underperforms in terms of RSSI compared to higher SF. The negative impact of additional floors on signal quality causes LAP to transmit at maximal power and thus allows for longer distances to be covered on the first floor. Distances between 36.81 m and 141.84 m can be observed within a

single floor for all SF but quickly lose signal strength for each extra floor by nearly halving the reachable distance per additional floor. Depending on the SF, the maximal number of reachable floors varies from 4 to 15. However, we observe that after 5 floors the area covered in a floor by the signal is substantially reduced under any SF. Fig. 11 compares our model output with the received signal data at each gateway. We find that our model accurately identifies strong signal strength but underestimates how long a viable but weak signal can be received. The remote third gateway remained outside of our model's boundary with its reception of transmissions and exhibited generally lower SNR and RSSI. In general, we observed that increasing the DR (SF8-SF12) allowed for longer ranges similar to outdoor applications, but the signal quickly diminished across distance and with every additional floor. An exception was SF7 which overperformed in SNR but underperformed in RSSI possibly due to ADR.

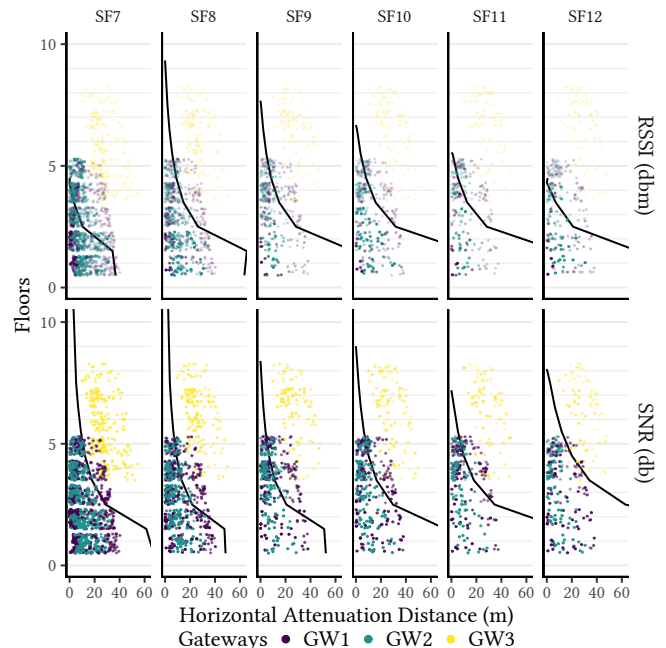


Fig. 11. Received data quality by floor (3.36 m per floor), distance, and gateway. Different colors for each graph represent different gateways (purple: 1; jade: 2; yellow: 3). The black curves show the boundary where the models predict that transmissions occur below the noise floor. Each point represents a sensor-gateway connection, the opacity represents the average signal quality, and the size depends on the number of transmissions received at a gateway compared to the number of transmissions received by the other gateways.

V. DISCUSSION

While the use of indoor LoRaWAN has been previously advocated, research has failed to deliver large scale applications, leaving a gap between the expectation and its realization. To our knowledge, this is the first project to deploy a LoRaWAN DISN and demonstrate its feasibility beyond theoretical models and ns-3 simulations [49]–[51]. We collected a large data set with more than 14 million transmissions (from 390 sensors over approximately 5 months) compared to (at most)

TABLE V
SNR AND RSSI LIMITS FOR TRANSMISSION IN OUR SYSTEM BASED ON MIXED MODELS

Max. reachable	SNR						RSSI					
	SF7	SF8	SF9	SF10	SF11	SF12	SF7	SF8	SF9	SF10	SF11	SF12
Distance 0 floors up	64.88 m	47.29 m	50.96 m	72.6 m	83.34 m	141.84 m	36.81 m	63.49 m	71.1 m	82.14 m	79.3 m	69.65 m
Distance 1 floor up	59.5 m	46.39 m	49.73 m	70.87 m	82.73 m	141.59 m	34.36 m	65.4 m	74.49 m	88.78 m	85.46 m	72.69 m
Distance 2 floors up	27.85 m	20.96 m	21.01 m	30.98 m	33 m	57.66 m	10.4 m	26.48 m	28.42 m	31.8 m	28.34 m	21 m
Distance 3 floors up	17.19 m	12.76 m	11.96 m	18.26 m	17.79 m	31.89 m	3.43 m	14.72 m	14.9 m	15.72 m	12.6 m	7.1 m
Distance 4 floors up	11.84 m	8.7 m	7.53 m	11.99 m	10.43 m	19.38 m	0.11 m	9.03 m	8.44 m	8.13 m	5.24 m	0.64 m
Distance 5 floors up	8.61 m	6.29 m	4.89 m	8.27 m	6.07 m	11.99 m	-*	5.69 m	4.66 m	3.71 m	0.96 m	-*
Floors	14.82	15.25	9.87	11.74	8	8.68	4.26	9.33	7.68	6.68	5.55	4.31

Note:

* No meaningful output.

a couple thousand transmissions reported in previous research [20]. Consequently, we were able to assess the specific real world factors that affected our LoRaWAN DISN.

Previous research has focused on descriptive data for the distance limits of specific scenarios that provide some indication of the limitations of such systems [20], [21]. In some cases, theoretical models were developed to qualify these descriptions, but it is difficult to extend these models to other building structures and obstacles [16], [18], [47]. Distance to the gateway is a key metric for LoRaWAN networks performance in both indoor and outdoor applications. Outdoor applications with minimal interference are typically evaluated with respect to signal attenuation in different environments (e.g., rural versus urban) at the scale of kilometers. In contrast, signal attenuation indoors is at the scale of hundreds of meters because of building structures (e.g., walls and floors) causing shadowing and multi-path fading [14].

We investigated the limits of LoRaWAN indoors by applying a mixed model to represent signal attenuation and estimated the impact of different building and network characteristics on signal strength. Our model predicted that the signal could be transmitted between 36.81 m and 141.84 m (depending on SF) within the same floor (see Table IV) with the caveat that we had no transmissions beyond 64 m. Notably, this estimate is considerably lower than what has been previously reported [20], [21], [24]. The maximal distance further decreased if floor levels are also considered. Here, our model predicted a maximum coverage of 4 to 15 floors (depending on SF) directly above the gateway or at most 51.24 m upwards with the caveat that we had no transmissions beyond 8 floors. It appears that each additional floor upwards roughly halves the signal strength so that coverage on the fifth floor is already below 12 m on any SF. Our findings contrast with previous reports of a negligible effect of floors on signal strength [20] and extrapolations that a coverage of one gateway every 10 floors is manageable [15]. When comparing our model with the network data, we noticed that the remote gateway is outside of our area of high quality transmission (yellow in Fig. 11) and also has a FER of 80.55%, indicating a useful correlation between our model's predictions and the ability to receive transmissions.

Furthermore, we may have underestimated the impact of construction materials on signal strength because many messages were sent barely above the noise floor of SNR and RSSI due to the way in which ADR manages SF by selecting only higher SF on short distances when signal strength is weak. This could result in a biased sample of higher SF. These results also need to be interpreted carefully because linear modeling of the attenuation in a building may not be sufficient. As construction materials for floors and exterior walls vary from building to building, they impose constraints on the network. These constraints are difficult to generalize without computationally expensive simulations or large studies on the effects of different complex structures on signal quality. Despite these caveats, we believe to have found a conservative boundary for the deployment of DISNs and strongly recommend the use of multiple gateways placed every 30 m and 5 floors to ensure that as many transmissions as possible are received.

Another major source of discussion for the usability of LoRaWAN DISN is the loss of transmissions. While LoRaWAN is more robust than many other communication technologies, there is a limit on how many messages can be transmitted at the same time. With our setup (1.5 transmission per second), we observed only 1 to 5 colliding concurrent messages, accounting for 0.29% of all transmissions. Overall, we lost 8.06% of transmissions. We found that multiple gateways have mitigated the loss of transmissions, either due to environmental factors or network issues such as concurrency. Notably, our use of the third remote gateway provided two important lessons. First, our use of this gateway demonstrated how distances longer than 30 m across multiple floors led to a severe loss in capacity, as indicated by considerably worse FER (80.55%). Second, despite the weak contribution to overall transmission, this gateway still reduced the overall FER per sensor node by 1.31% compared to having only two gateways.

SF is usually an important factor to consider for the quality of a LoRaWAN network. However, in our setup, the ADR compels our network to use SF7 for 93% of transmissions because SF7 provides the highest data throughput at the lowest battery cost. This finding aligns with theoretical expectations that, for short distances, lower SF are more effective. Contrary to expectations, larger SF can actually improve signal quality

over shorter distances. Interestingly, indoors, the larger SF only provides up to twice the distance coverage of SF7 which contrasts starkly with the performance gain in outdoor scenarios. For indoor application, we would recommend to develop an ADR that also switches to a higher SF as long as the required data throughput can be maintained. If only standard ADR is available, our distance and floor recommendations (30 m; 5 floors) ensure a high quality signal throughout a building regardless of the chosen SF.

VI. CASE STUDY – HUMAN PRESENCE DURING THE COVID19 LOCKDOWN IN SPRING 2020

The core focus of this paper was on the feasibility of the network infrastructure. However, while testing the network, we also collected a large data set that continues to increase by 250,000 data points every day. Between March 8th and August 4th (2020), our prototype collected 23.2 million data points (see Fig. 12). Before data collection, 137 sensors were installed, but due to COVID-19, the installation of the remaining 253 sensors was delayed until mid-May. Fig. 13 presents select sensor data in 24-hour cycles aggregated by room over the whole period for the second floor.

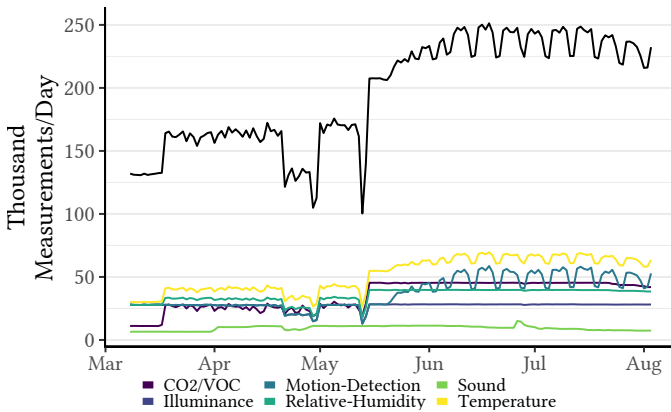


Fig. 12. Measurements per sensor type and day. The total is shown in black. Lower number of measurements before mid May are due to the Covid19-related lockdown delaying sensor installation.

While a ground truth data set (i.e., number of people counted) could not yet be generated to validate human presence models, we use the COVID-19-related lockdown to investigate whether variations in the sensor data can indicate human presence. We summarize the sensor data at the room level as variance indicators $\mathbb{V}_{r,t}$ (see Eq. 3), which aggregate data by room r and hour t based on the sensor type i and the individual sensor device j . Because of the different scales of these measurements, we use z-scores by sensor type i so that each measurement v_{r,i,j,t_k} is aggregated over all j devices in a room r and measurements k in time slot t (see Eq. 2). As some extraordinary events (e.g., construction with noise up to 14 times louder than average) have resulted in extreme outliers, we limited measures to within 3 standard deviations and then aggregated with respect to sensor type i (see Eq. 3).

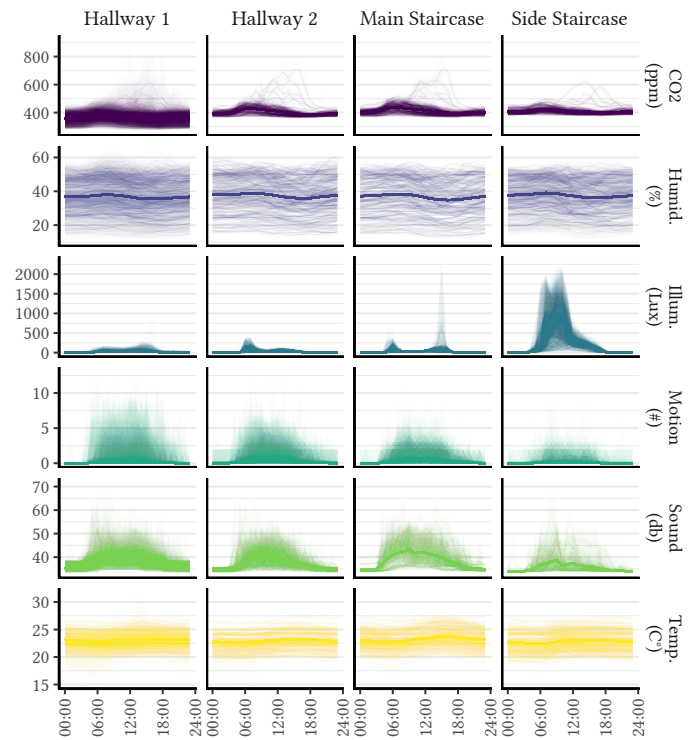


Fig. 13. Sensor data on the second floor. The soft lines indicate the values for each day. The strong line indicates the average over all days. The shaded areas represent the range between the minimal and maximal values measured.

$$\tilde{\mathbb{V}}_{r,i,t} = \frac{1}{n_{r,i}} \sum_{j,k} \frac{v_{r,i,j,t_k} - \bar{v}_i}{\sigma_{v_i}} \quad (2)$$

$$\mathbb{V}_{r,t} = \frac{1}{n_r} \sum_i \max\left(-3, \min\left(3, \tilde{\mathbb{V}}_{r,i,t}\right)\right) \quad (3)$$

Our variance indicator allows us to observe strong periodic variation in each room and to tentatively attribute portions of the variation to human presence. See Fig. 14 for our analysis of the ground floor. Because of the COVID-19 lockdown at the beginning of the study, we were able to attribute some of the later variations to returning human presence by marking key events that occurred inside the building. On March 13th, the lockdown was enacted, and until April 22nd, only essential personnel (e.g., building management and reception) were still present. From April 22nd to June 8th, a slight easing of the lockdown was introduced that allowed some researchers to return with special permits. From June 8th to August 3rd, all researchers were allowed back in the building. From August 3rd onwards, the building was again opened to the public with students and visitors allowed to enter without special permits. The strongest impact on variations in the data was when presence was strongly reduced during the first lockdown period. This is most visible in the Side Staircase, Hallways 1 & 3, and to a lesser degree in Hallway 2. Two major exceptions were the Main Staircase and the Lobby where the offices of essential personnel are located. After the special

permits were issued, some presence returned to the building, producing additional variation. When full access was restored for researchers, a regular pattern in variation returned.

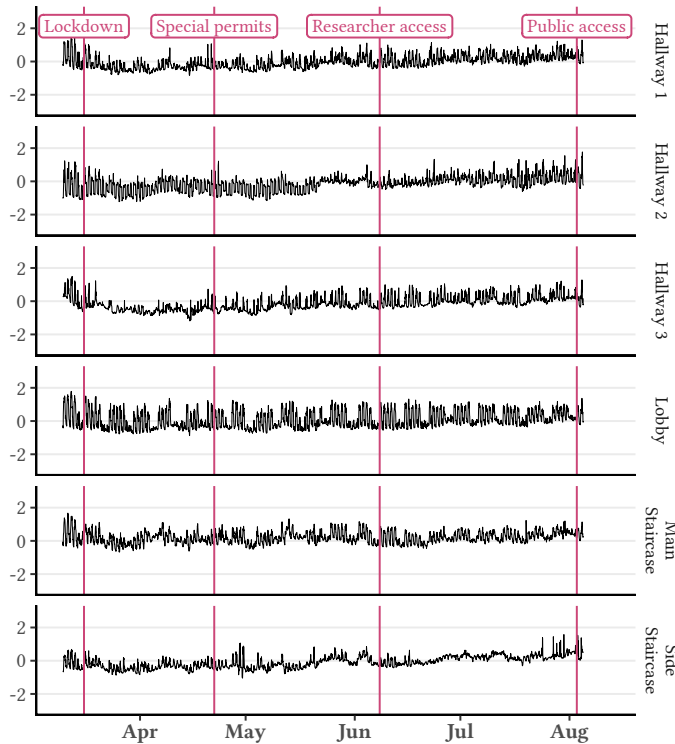


Fig. 14. Sensor data aggregated by hour and room for the ground floor. The variance indicator represents variation up to ± 3 standard deviations. The magenta lines indicate key events related to the Covid-19 lockdown.

Analyzing human presence indoors can be a difficult but useful endeavor for researchers, designers, and planners. This new and rich data set of environmental characteristics from a real building will allow us to develop novel applications for analyzing the impact of human presence in an enclosed public space. While we lacked ground truth measurements to validate any kind of occupancy model, we benefited from the natural experiment resulting from the COVID-19-lockdown. This allowed us to observe patterns of variation in the data that could only be explained by the sudden absence of human presence in the building over an extended period of time. Our immediate next steps will be to compile a ground truth data set for human presence against which we will be able to run more complex models that can spatially describe human activity within a building. Towards this end, we will use automated visitor counts and localization derived from videos.

While accuracy is expected to be much lower with passive tracking compared to active tracking, our approach benefits from the preservation of privacy, measures that are not biased by sampling, and the observation of more natural user behavior. Passive tracking elegantly circumvents the privacy issue by estimating changes in environmental measurements and “naturally aggregating” data from stationary sensors without reference to the users’ individual identities. Our approach can also reduce bias in modeling human activity in a building be-

cause we account for the whole population of a building rather than convenience samples of people who allow active tracking. Finally, the passive nature of the system also allows us to observe more natural behavior from building users reducing the observer effects that can occur with active tracking.

VII. CONCLUSION

Despite the potential for fine-grained data indoors, previous work has focused on demonstrating the possibility of creating proof-of-concept systems by relying on few sensor nodes or simulations without a dense network implementation. We built the first LoRaWAN DISN that extends LoRaWAN’s appeal beyond its initial technical scope of long range low power applications. Indoor environments attenuate the LoRaWAN signal at a quicker rate compared to outdoor scenarios, and previous estimates for indoor ranges of 200 m to 600 m seem optimistic [21], [24]. In contrast, our system achieved good coverage up to 30 m with an upper bound around 141 m at SF12. Higher SFs improve signal quality but only marginally increase distance coverage to up to twice that of SF7 due to signal shadowing and multi-path fading. Similarly, the impact of floors on signal quality resulted in nearly halving of reachable distance per additional floor. To our knowledge, this is the first validation of previous simulation research using multiple gateways [50]. We demonstrated their positive impact by recovering up to 37.5% of lost messages in real-world conditions. Our recommendation focuses on obtaining the strongest possible signal while minimizing energy costs at the nodes and data loss. Specifically, we recommend the placement of one LoRaWAN gateway every 30 m and 5 floors. A denser gateway placement is critical to the deployment of LoRaWAN DISNs, more similar to placing WiFi-routers than outdoor LoRaWAN gateways. While LoRaWAN’s performance on average may approximate technologies such as WiFi under optimal conditions (at 45 m), the energy consumption of LoRaWAN devices is lower and they not require wires. We believe that, for pure sensing applications, LoRaWAN offers many advantages and can help to increase sensing density in buildings while keeping maintenance costs low. Our next steps are extending the research on LoRaWAN DISNs and passively sensing human presence with a DT. We will develop variations of ADR. We will also expand this prototype into a fully-fledged DT platform that enables predictions, statistical modeling, user studies [40], and agent simulations [41].

ACKNOWLEDGMENT

This research is funded by grant ETH-15 16-2 and supported by OrbiWise with hard- and software. We thank Michal Gath-Morad for the BIM and Axel Beckert for feedback.

REFERENCES

- [1] U. Raza, P. Kulkarni, and M. Sooriyabandara, “Low power wide area networks: An overview,” *IEEE Commun. Surveys Tuts.*, vol. 19, no. 2, pp. 855–873, 2017.
- [2] M. C. Vuran, A. Salam, R. Wong, and S. Irmak, “Internet of underground things in precision agriculture: Architecture and technology aspects,” *Ad Hoc Netw.*, vol. 81, pp. 160–173, 2018.

- [3] M. Lloriot, A. Aljer, and I. Shahrouh, "Analysis of the use of LoRaWAN technology in a large-scale smart city demonstrator," in *Sens. Netw. Smart and Emerg. Technol. (SENSET)*, 2017. New York: IEEE, 2017.
- [4] M. Saravanan, A. Das, and V. Iyer, "Smart water grid management using lpwan iot technology," in *2017 Global Internet of Things Summit (GIoTS)*. IEEE, 2017.
- [5] N. Varsier and J. Schwoerer, "Capacity limits of lorawan technology for smart metering applications," in *2017 IEEE Int. Conf. Commun. (ICC)*. IEEE, 2017.
- [6] M. T. Lazarescu, "Design of a wsn platform for long-term environmental monitoring for iot applications," *IEEE Trans. Emerg. Sel. Topics Circuits Syst.*, vol. 3, no. 1, pp. 45–54, 2013.
- [7] N. Sornin, "LoRaWAN 1.1 Specification," LoRa Alliance, Tech. Rep., 2017. [Online]. Available: <https://loro-alliance.org/>
- [8] K. Mekki, E. Bajic, F. Chaxel, and F. Meyer, "A comparative study of lpwan technologies for large-scale iot deployment," *ICT express*, vol. 5, no. 1, 2019.
- [9] A. Berni and W. Gregg, "On the utility of chirp modulation for digital signaling," *IEEE Trans. Commun.*, vol. 21, no. 6, pp. 748–751, 1973.
- [10] Semtech Corporation, "AN1200.22 LoRa Modulation Basics," Semtech Corporation, Camarillo, CA, Tech. Rep., 2015.
- [11] IEEE Comput. Soc., "IEEE Standard 802.15.4a-2007," IEEE, New York, Tech. Rep., 2007.
- [12] ETSI, "ETSI EN 300 220-2 V3.2.1," ETSI, Tech. Rep., 2018.
- [13] N. Abramson, "The aloha system: Another alternative for computer communications," in *Proc. Fall Joint Comput. Conf. (AFIPS)*. New York: ACM, 1970, p. 281–285.
- [14] E. D. Ayele, C. Hakkenberg, J. P. Meijers, K. Zhang, N. Meratnia, and P. J. Havinga, "Performance analysis of lora radio for an indoor iot applications," in *2017 Int. Conf. Internet of Things for the Global Community (IoTGC)*. New York: IEEE, 2017.
- [15] M. Centenaro, L. Vangelista, A. Zanella, and M. Zorzi, "Long-range communications in unlicensed bands: The rising stars in the iot and smart city scenarios," *IEEE Trans. Wireless Commun.*, vol. 23, no. 5, pp. 60–67, 2016.
- [16] M. M. Erbati, G. Schiele, and G. Batke, "Analysis of lorawan technology in an outdoor and an indoor scenario in duisburg-germany," in *2018 3rd Int. Conf. Comput. and Commun. Syst. (ICCCS)*. New York: IEEE, 2018, pp. 273–277.
- [17] L. Gregora, L. Vojtech, and M. Neruda, "Indoor signal propagation of lora technology," in *17th Int. Conf. Mechatronics-Mechatronika*. New York: IEEE, 2016.
- [18] J. Haxhibeqiri, A. Karaagac, F. Van den Abeele, W. Joseph, I. Moerman, and J. Hoebeke, "Lora indoor coverage and performance in an industrial environment: Case study," in *22nd IEEE Int. Conf. Emerg. Technol. Factory Autom. (ETFA)*. New York: IEEE, 2017.
- [19] M. I. Muzammir, H. Z. Abidin, S. A. C. Abdullah, and F. H. K. Zaman, "Performance analysis of lorawan for indoor application," in *9th IEEE Symp. Comput. Appl. & Ind. Electron. (ISCAIE)*. New York: IEEE, 2019, pp. 156–159.
- [20] P. Neumann, J. Montavont, and T. Noël, "Indoor deployment of low-power wide area networks (LPWAN): A LoRaWAN case study," in *12th IEEE Int. Conf. Wireless and Mobile Comput., Netw. and Commun. (WiMob)*. New York: IEEE, 2016.
- [21] J. Petäjäjärvi, K. Mikhaylov, R. Yasmin, M. Hämäläinen, and J. Iinatti, "Evaluation of LoRa LPWAN technology for indoor remote health and wellbeing monitoring," *Int. J. of Wireless Inf. Netw.*, vol. 24, no. 2, pp. 153–165, 2017.
- [22] N. Vatcharatiensakul, P. Tuwanut, and C. Pornavalai, "Experimental performance evaluation of lorawan: A case study in bangkok," in *14th Int. Joint Conf. Comput. Science and Softw. Eng. (JCSSE)*. New York: IEEE, 2017.
- [23] T. Wendt, F. Volk, and E. Mackensen, "A benchmark survey of long range (lora) spread-spectrum-communication at 2.45 ghz for safety applications," in *16th IEEE Annu. Wireless and Microw. Technol. Conf. (WAMICON)*. New York: IEEE, 2015.
- [24] P. J. Radcliffe, K. G. Chavez, P. Beckett, J. Spangaro, and C. Jakob, "Usability of LoRaWAN technology in a central business district," in *85th IEEE Veh. Technol. Conf. (VTC)*. New York: IEEE, 2017.
- [25] K.-C. Lai, B.-H. Ku, and C.-Y. Wen, "Using cooperative pir sensing for human indoor localization," in *27th Wireless and Optical Commun. Conf. (WOCC)*. New York: IEEE, 2018, pp. 1–5.
- [26] M. Moussaïd, V. R. Schinazi, M. Kapadia, and T. Thrash, "Virtual sensing and virtual reality: How new technologies can boost research on crowd dynamics," *Front. Robot. and AI*, vol. 5, 2018.
- [27] P. Kiefer, I. Giannopoulos, and M. Raubal, "Where am i? investigating map matching during self-localization with mobile eye tracking in an urban environment," *Trans. GIS*, vol. 18, no. 5, pp. 660–686, 2014.
- [28] W. Wang, J. Chen, and T. Hong, "Occupancy prediction through machine learning and data fusion of environmental sensing and Wi-Fi sensing in buildings," *Autom. Constr.*, vol. 94, pp. 233–243, 2018.
- [29] M. Batty, "Digital twins," *Environment and Planning B*, vol. 45, no. 5, pp. 817–820, 2018.
- [30] N. Mohammadi and J. E. Taylor, "Smart city digital twins," in *IEEE Symp. Series Int. Computational Intelligence (SSCI)*. Honolulu, Hawaii: IEEE, 2017, pp. 1–5.
- [31] M. Bell, "Service-oriented modeling," *John Wiley & Sons, Inc*, 2008.
- [32] M. Grieves and J. Vickers, "Digital twin: Mitigating unpredictable, undesirable emergent behavior in complex systems," in *Transdisciplinary Perspectives Complex Systems*. Heidelberg: Springer, 2017, pp. 85–113.
- [33] F. Tao, H. Zhang, A. Liu, and A. Nee, "Digital twin in industry: State-of-the-art," *IEEE Trans. Ind. Inform.*, vol. 15, pp. 2405–2415, 2018.
- [34] J. Jiang, M. Tobia, R. Lawther, D. Branchaud, and T. Bednarz, "Double vision: Digital twin applications within extended reality," in *ACM SIGGRAPH 2020 Appy Hour*, 2020, pp. 1–2.
- [35] D. K. Hamilton and D. H. Watkins, *Evidence-based design for multiple building types*. John Wiley & Sons, 2009.
- [36] T. Polonelli, D. Brunelli, A. Marzocchi, and L. Benini, "Slotted aloha on lorawan-design, analysis, and deployment," *Sensors*, vol. 19, no. 4, p. 838, 2019.
- [37] J. C. Liando, A. Gamage, A. W. Tengourtius, and M. Li, "Known and unknown facts of lora: Experiences from a large-scale measurement study," *ACM Trans. Sens. Netw.*, vol. 15, no. 2, pp. 1–35, 2019.
- [38] M. Sauter, *From GSM to LTE-advanced: an introduction to mobile networks and mobile broadband*. John Wiley & Sons, 2014.
- [39] E. Borgia, "The Internet of Things vision: Key features, applications and open issues," *Comput. Commun.*, vol. 54, pp. 1–31, 2014.
- [40] J. Grübel, R. Weibel, M. H. Jiang, C. Hölscher, D. A. Hackman, and V. R. Schinazi, "Eve: A framework for experiments in virtual environments," in *Spatial Cogn. X*. Heidelberg: Springer, 2016, pp. 159–176.
- [41] M. Gath-Morad, L. Aguilar, R. C. Dalton, and C. Hölscher, "cogarch: Simulating wayfinding by architecture in multilevel buildings," in *11th Annu. Symp. Simulation for Architecture & Urban Design (SimAUD 2020)*. New York: ACM, 2020, pp. 27–34.
- [42] C. Jiang, M. K. Masood, Y. C. Soh, and H. Li, "Indoor occupancy estimation from carbon dioxide concentration," *Energy and Buildings*, vol. 131, pp. 132–141, 2016.
- [43] Z. Yang and B. Becerik-Gerber, "Modeling personalized occupancy profiles for representing long term patterns by using ambient context," *Building and Environment*, vol. 78, pp. 23–35, 2014.
- [44] P. Liu, S. Nguang, and A. Partridge, "Occupancy Inference Using Pyroelectric Infrared Sensors Through Hidden Markov Models," *IEEE Sensors J.*, vol. 16, no. 4, pp. 1062–1068, 2016.
- [45] Orbiwise, "OrbiLINK," Orbiwise, Geneva, Tech. Rep., 2018.
- [46] L. Richardson, M. Amundsen, M. Amundsen, and S. Ruby, *RESTful Web APIs: Services for a Changing World*. O'Reilly Media, 2013.
- [47] J. Petäjäjärvi, K. Mikhaylov, A. Roivainen, T. Hanninen, and M. Pettisalo, "On the coverage of lpwans: range evaluation and channel attenuation model for lora technology," in *14th Int. Conf. ITS Telecommun. (ITST)*. IEEE, 2015, pp. 55–59.
- [48] D. Bates, M. Mächler, B. Bolker, and S. Walker, "Fitting linear mixed-effects models using lme4," *J. of Statistical Softw.*, vol. 67, no. 1, pp. 1–48, 2015.
- [49] D. Magrin, M. Centenaro, and L. Vangelista, "Performance evaluation of lora networks in a smart city scenario," in *IEEE Int. Conf. Commun. (ICC)*, 2017, pp. 1–7.
- [50] F. Van den Abeele, J. Haxhibeqiri, I. Moerman, and J. Hoebeke, "Scalability analysis of large-scale lorawan networks in ns-3," *IEEE Internet of Things J.*, vol. 4, no. 6, pp. 2186–2198, 2017.
- [51] N. Matni, J. Moraes, H. Oliveira, D. Rosário, and E. Cerqueira, "Lora-wan gateway placement model for dynamic internet of things scenarios," *Sensors*, vol. 20, no. 15, p. 4336, 2020.